Wu *et al. Earth, Planets and Space* (2022) 74:7
https://doi.org/10.1186/s40623-021-01560-8

Earth, Planets and Space

FULL PAPER Open Access

Characteristics of landslides triggered by the 2013 M_L6.5 Nantou, Taiwan, earthquake

Bing Sheng Wu[1], Ray Y. Chuang[2,3*], Yi-Chin Chen[4] and Ya-Shien Lin[2]

Abstract

Earthquake-triggered landslides are common disasters of active mountain belts. Due to the lack of earthquake-triggered landslide inventory in Taiwan, it is not intuitive to observe spatial relationships and discover unique patterns between landslides and essential triggers. We examined strong earthquake events in Taiwan after the 1999 M_w7.6 Chi-Chi earthquake and targeted the 2013 M_L6.5 Nantou earthquake to create the landslide inventory. We adopted two Landsat-8 satellite images before and after the event to detect landslides, and incorporated a 20-m DEM and rock type data of Taiwan to represent key factors triggering earthquake-induced landslides such as peak ground acceleration (PGA), lithology, slope roughness, slope, and aspect. Based on the analysis of the density of landslides, there are strong correlations between the landslide occurrence and seismic and geomorphic factors. Furthermore, we noticed that the landslide aspects have a systematic tendency towards the northeast, which is not correlated with the dip directions and wave propagation directions. Instead, we found that the northeastward landslide aspect is more associated with the westward–southwestward surface movement at the landslides. We found that the included angles between the landslide aspects and the displacement directions for all the landslides are ~100°–180°. The relationship indicated that the coseismic deformation of the Nantou earthquake may play a role in the landslide distribution.

Keywords: Earthquake-induced landslides, Coseismic deformation, Mass movement, Landslide aspect

Graphical Abstract

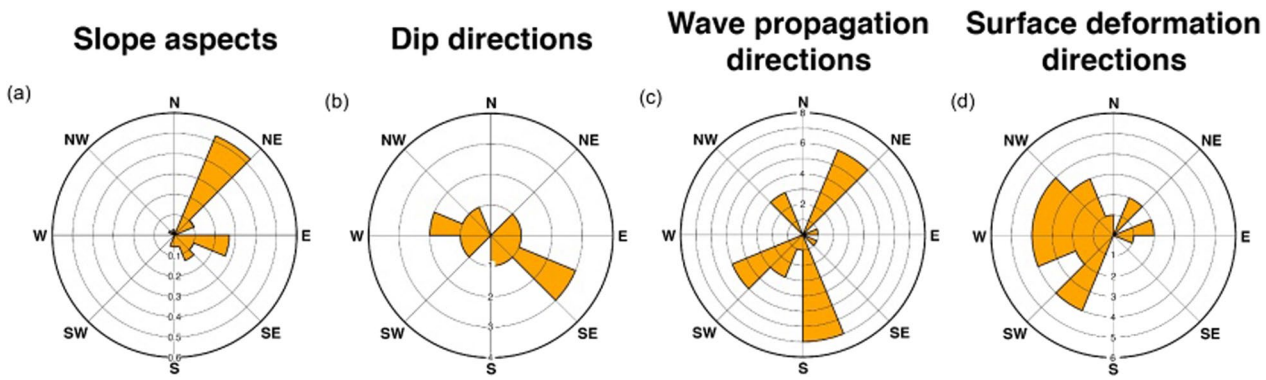

*Correspondence: raychuang@ntu.edu.tw
[2] Department of Geography, National Taiwan University, Taipei, Taiwan
Full list of author information is available at the end of the article

Introduction

Earthquake-triggered landslides are important disasters, which can cause fatalities (Marano et al. 2009; Daniell et al. 2017; Nowicki Jessee et al. 2020) and further surface processes influencing geomorphic evolution (e.g., Chuang et al. 2020; Fan et al. 2019). In order to understand driving factors of earthquake-triggered landslides (e.g. Keefer 1984, 2002; Khazai and Sitar 2004; Meunier et al. 2007; Tibaldi et al. 1995), it is essential to have the inventories of earthquake-triggered landslides for the analyses (Harp et al. 2011; van Westen et al. 2006). The landslide datasets can be used to analyze the relationship between the landslide occurrence and the seismic and geologic factors. In addition, the landslide datasets can serve as the training data for susceptibility assessments and real-time prediction (e.g., Chuang et al. 2021; Budimir et al. 2015; Nowicki Jessee et al. 2018). The inventories rely on mapping results for individual seismic events, and global inventories have been progressively compiled (Keefer 1984; Rodriguez et al. 1999; Schimitt et al. 2017; Tanyaş et al. 2017). It is important to keep generating such inventories to have a more comprehensive database of earthquake-triggered landslides.

Among landslide hotspots in the world (Nadim et al. 2006), the island of Taiwan is subject to abundant earthquakes and heavy rainfalls. Accordingly, landslides occur frequently in Taiwan, and it is critical to map landslides in Taiwan after large seismic or rainfall events. Especially, the Taiwan orogenic belt is formed under the strong plate convergence between the Eurasian and Philippine Sea plates with numerous seismogenic structures (e.g., Shyu et al. 2005, 2020) and frequent earthquakes (e.g., Wu et al. 2008) across the orogenic belt, causing high seismic potential (Chan et al. 2020; Shyu et al. 2005). In the recent 2 decades, several $M>6$ earthquakes in Taiwan occurred in the mountain belt and indeed caused significant hazards and distributed landslides. Compared to rainfall-induced landslides (Lee and Fei 2015; Lin et al. 2017), however, earthquake-induced landslides in Taiwan are less mapped and analyzed. To date, only a couple of earthquake events, the 1998 M_L6.2 Jueili earthquake and the 1999 M_w7.6 Chi-Chi earthquake, have comprehensive landslide inventories (Huang and Lee 1999; Liao and Lee 2000). The Chi-Chi earthquake generated more than 9000 landslides (Liao and Lee 2000). Therefore, we examined all the $M>6$ on-land earthquakes after the Chi-Chi earthquake and targeted the 2013 M_L6.5 Nantou earthquake to analyze its earthquake-triggered landslides.

In this study, we aimed to map earthquake-triggered landslides of the Nantou earthquake and to analyze the relationship between the landslide distribution and seismic and environmental factors. The 2013 M_L6.5 Nantou earthquake is one of the strong earthquakes after the Chi-Chi earthquake that has reported coseismic landslides. The Nantou earthquake occurred in the most active part of the Taiwan orogen, which also lies within the damaged area of the Chi-Chi earthquake. Therefore, the analysis will help us to better understand the characteristics of earthquake-triggered landslides of the active Taiwan orogenic belt.

Study area

The study area of this research is at the Nantou County, the central part of Taiwan, which is also the center of the Taiwan mountain belt (Fig. 1). The epicenter of the 2013 M_L6.5 Nantou earthquake is close to the Lishan fault, a boundary between the Central Range to the east and Hsuenshan Range to the west. The Nantou area experienced severe damage during the 1916 Nantou earthquake sequence (Cheng et al. 1999). Almost a century later, the M_w7.6 Chi-Chi earthquake struck central Taiwan with widespread coseismic landslides (Liao and Lee 2000). Especially, there were several $M_w>5.8$ aftershocks of the Chi-Chi earthquake that occurred in the study area. The landslides transiently increased landslide rates (Chang et al. 2007) and sediment discharge (Dadson et al. 2004; Hovius et al. 2011) around central Taiwan for ~6 years. After the increased landslides and sediment delivery were diminished, two strong earthquakes in 2013, the M_L6.2 Nantou earthquake in March and the M_L6.5 Nantou earthquake in June, occurred to the east of the Chi-Chi earthquake in the study area (Fig. 1). The two earthquakes had no surface rupture, but the second earthquake produced larger surface displacements (Chuang et al. 2013) and ground shaking with scattered landslides. Geodetic inversions suggested that the two earthquakes occurred on the same east-dipping mid-crust fault (Chuang et al. 2013). Source inversions showed that the earthquakes had distinct directivity effects, indicating stress heterogeneity in this area (Lee et al. 2015; Wen et al. 2014). The M_L6.5 Nantou earthquake with the landslides occurred within the damaged area of the Chi-Chi earthquake and drew local people's attention. Therefore, in this study, we used satellite imagery to map the landslides induced by the earthquake and analyzed what controlled the landslides of this seismic event.

Material and methods

This study focused on the use of remote sensing data for mapping earthquake-triggered landslides and the spatial relationship between landslides and key triggers. First, we screened earthquake events that have high magnitude and impacts on the Taiwan island followed the criteria below: (1) it happened after the Chi-Chi earthquake on September 21, 1999. (2) The magnitude of this event was larger than M_L6.0. (3) The epicenter was located on the

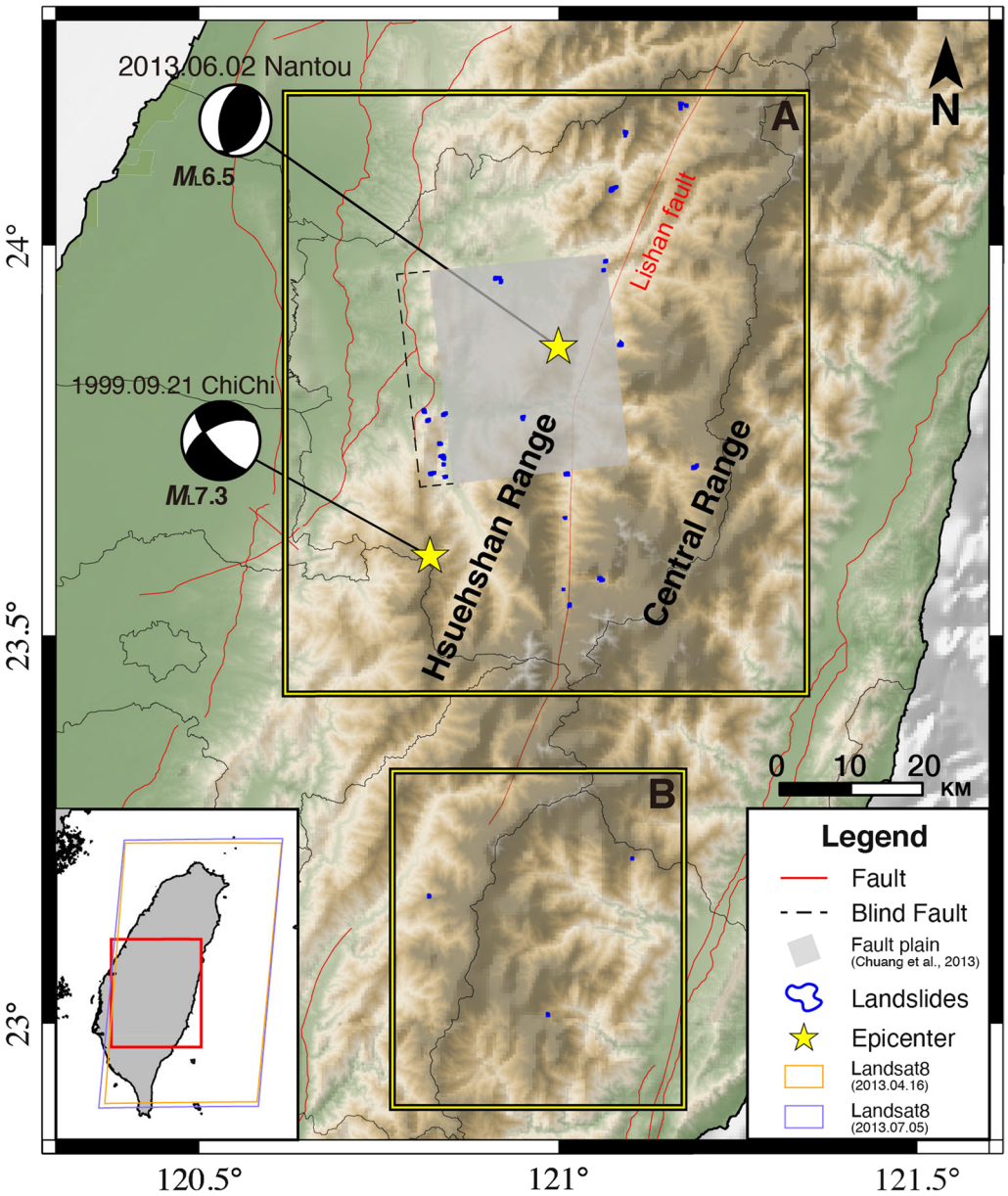

Fig. 1 Landslide areas for the 2013 M_L6.5 Nantou earthquake. Square **A**: the main extent of landslides. Square **B**: landslides might be triggered by the earthquake

island of Taiwan. (4) Landsat images before and after 2 or 3 months of an earthquake with cloud cover less than 10% could be identified. Based on these criteria, we chose the 2013 M_L6.5 Nantou earthquake in this study.

We used satellite imagery before and after the earthquake to map large earthquake-triggered landslides of the Nantou earthquake. The earthquake took place on June 2, 2013, and caused landslides and loss of human lives. The epicenter was 23.86°N, 120.97°E and the depth of the epicenter was 14.5 km. Since there is no landslide inventory for the 2013 Nantou earthquake, we conducted landslide detection through the use of remote sensing technologies. Two Landsat-8 images acquired on April 16, 2013, and July 5, 2013, were cloud-free, and we searched for large landslides within a 100-km radius of the epicenter. There was no heavy rainfall before the earthquake, so we excluded the influence of rainfall on the landslides (Additional file 1: Figure S1). The advantage of using Landsat imagery is twofold: (1) it is free-access open data, and (2) it has been broadly used in landslide detection for a large

area (e.g., Barlow et al. 2003; Deijns et al. 2020; Mantovani et al. 1996; Marcelino et al. 2009; Yu et al. 2020). Due to the spatial resolution of Landsat images, we did not identify landslide areas under 3600 m^2 (4 pixels) and focused on large landslides. We projected the pre- and post-earthquake images to the TWD97 projected coordinate system, which is the Taiwan datum defined in 1997 based on the GRS80 reference ellipsoid with respect to the ITRF94 at the epoch of the beginning of 1997 (Yang et al. 2001). The extraction of landslide areas required three types of spectrum bands from Landsat images: visible bands, infrared radiation bands, and Landsat Collection 1 Level-1 Quality Assessment Band. After the preparation of all images, we detected changes from both pre- and post-earthquake images to identify landslide areas and converted all the landslide areas to polygons data. All the vector-based landslide areas are converted to 20-m-resolution raster data for further analysis.

After we mapped landslides, we calculated the areas and volume of all landslides and analyzed the relationship between landslides and key factors that cause earthquake-triggered landslides. The relationship between area (A) and volume (V) of landslides is:

$$V = \alpha \times A^{\gamma}.$$

Since we cannot well distinguish the type of landslides from remote sensing imagery, we adopted the parameters of $\alpha = 0.146$ and $\gamma = 1.332 \pm 0.005$ for all landslide types from Larsen et al. (2010). After the detection of landslide areas, we examined the spatial relationship between the locations of landslides and key factors that caused earthquake-triggered landslides. Based on the statistical model for earthquake-triggered landslides in Taiwan (Chuang et al. 2021), key factors selected in this study were peak ground acceleration (PGA), lithology, slope roughness, slope, and aspect. PGA represents the seismic shaking of the earthquake. We accessed PGA data from the Central Weather Bureau (CWB), Taiwan and interpolated the point-based data to represent the degree of ground motion of the 2013 M_L6.5 Nantou earthquake. One seismic station MTN167 shows very high PGA over 1 g in the horizontal direction. Compared with the PGA values with other surrounding stations, the data of MTN167 may be an outlier. Therefore, we interpolated PGA based on the method of Hsiao (2007). Slope, slope roughness, and aspect are the topographic properties of the study area. Lithology is the rock type in Taiwan. We generated lithological data based on the classification of rock types based on the geologic map of Taiwan from the Central Geological Survey (CGS) (Central Geological Survey 2000). We used the 20-m digital elevation model (DEM) of Taiwan in ArcGIS 10.6 to calculate aspect and slope angle. We adopted the slope dataset for the calculation of slope roughness. Following previous studies (Budimir et al. 2015; Chuang et al. 2021), the value of slope roughness of each cell is calculated by the standard deviation of the slope with surrounding 8 cells (a 3×3 moving window). We categorized all data into different classes and overlaid landslide areas with each classified dataset to calculate the density of landslides. The density of landslides is the ratio between the total landslide area in one class and the total area of that class. We drew a chart to represent the density of landslides in each class from one dataset. The overlaid datasets and the statistical results were listed together to observe the spatial correlation of landslides and those triggering factors.

Results

We classified two Landsat images for the 2013 M_L6.5 Nantou earthquake and extracted 30 large earthquake-triggered landslides (Fig. 1). The total area of triggered landslide is 2.1353 km^2 and the total volume of landslide mass is 0.1728 ± 0.0007 km^3. We examined the mapped landslides of the 2013 Nantou earthquake and the landslide inventory of the 1999 Chi-Chi earthquake (Liao and Lee 2000), and we found that most of the mapped landslides are newly formed and only 10% of the mapped landslides are partially overlapped with the Chi-Chi earthquake landslides. In addition, since the increased landslide rate of the Chi-Chi earthquake is transient and decays to the background value in 4 years (Marc et al. 2015), we ignored the influence of the Chi-Chi earthquake on the mapped landslides.

The seismogenic fault of the Nantou earthquake is an east-dipping thrust fault (Chuang et al. 2013) and all of the mapped landslides are located in the hanging-wall area (Fig. 1), consistent with the observation that most landslides occur in the hanging-wall area for thrust-faulting earthquakes (Dai et al. 2011; Khazai and Sitar 2004; Sato et al. 2007; Yagi et al. 2009; Zhao et al. 2019). The number of the mapped large landslides in this study is small because the focal depth of the Nantou earthquake is deep and has no surface rupture, similar to the finding in previous studies that the number of landslides for such earthquakes can be significantly smaller than the one for shallow earthquakes with surface ruptures (e.g., Kargel et al. 2016).

We overlaid the landslides with each triggering factor and analyzed the spatial relationship between the landslides and these factors. Figure 2 shows the statistical results and spatial distribution of landslides. Firstly, as we stated in the previous section, we conducted spatial interpolation of PGA data based on a 0.1g interval (Fig. 2a). The mapped landslides occurred at places with PGA values greater than 0.2, which is reasonable for the threshold for earthquake-triggered landslides (e.g., Liao and Lee

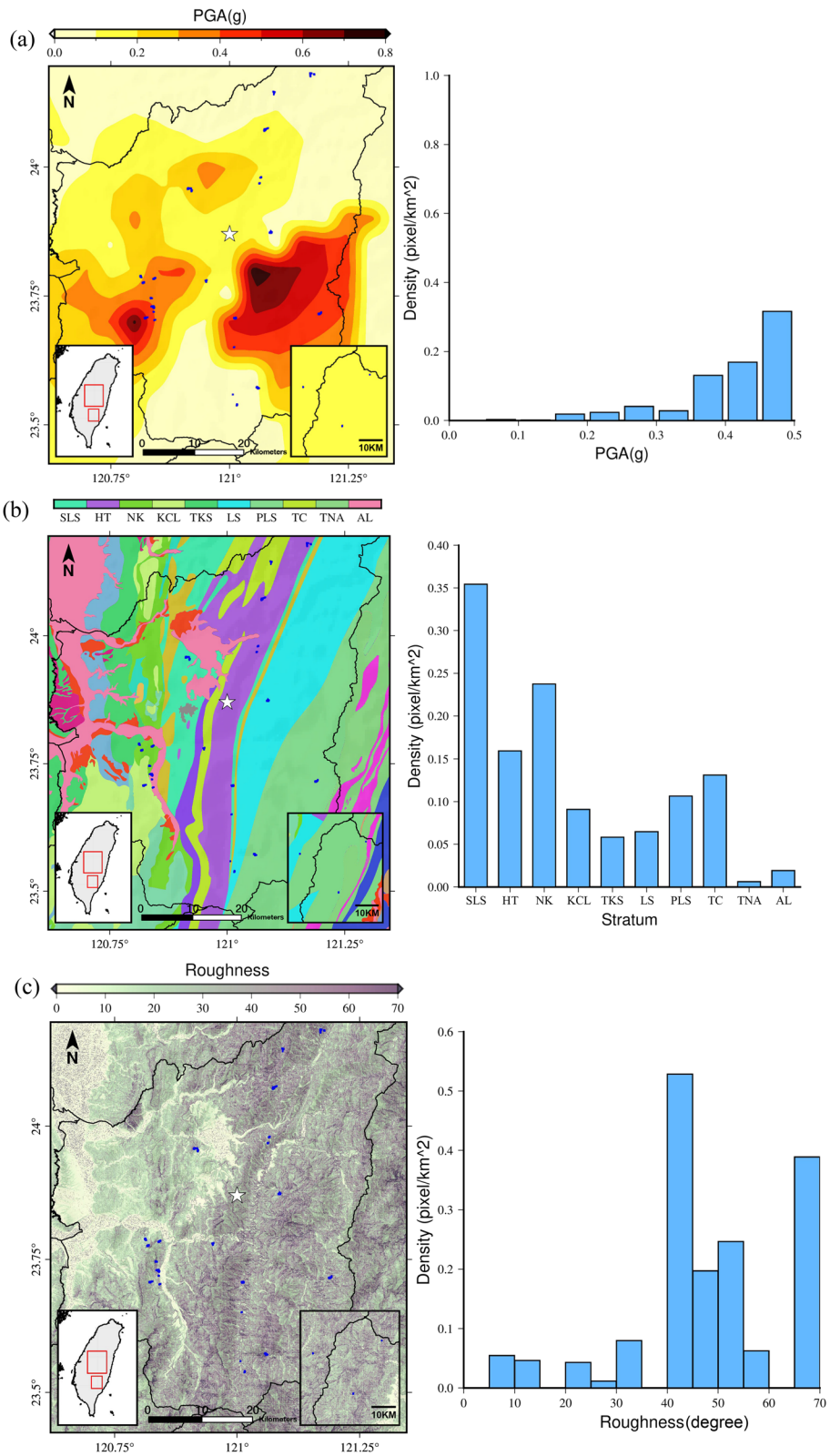

Fig. 2 Spatial correlations and bar charts between landslide densities and triggering factors: **a** PGA, **b** lithology, **c** slope roughness, **d** slope angle, and **e** aspect. Slope roughness: the standard deviation of the slope within a 3 × 3 cell window, *SLS* Szeleng Sandstone and Paileng Formation; *HT* Hsitsun Formation; *NK* Nankang Formation; *KCL* Kueichulin Formation; *TKS* Toukoshan Formation; *LS* Lushan Formation; *PLS* Pilushan Formation; *TC* Tachien Sandstone; *TNA* Tananao Schist; *AL* alluvium

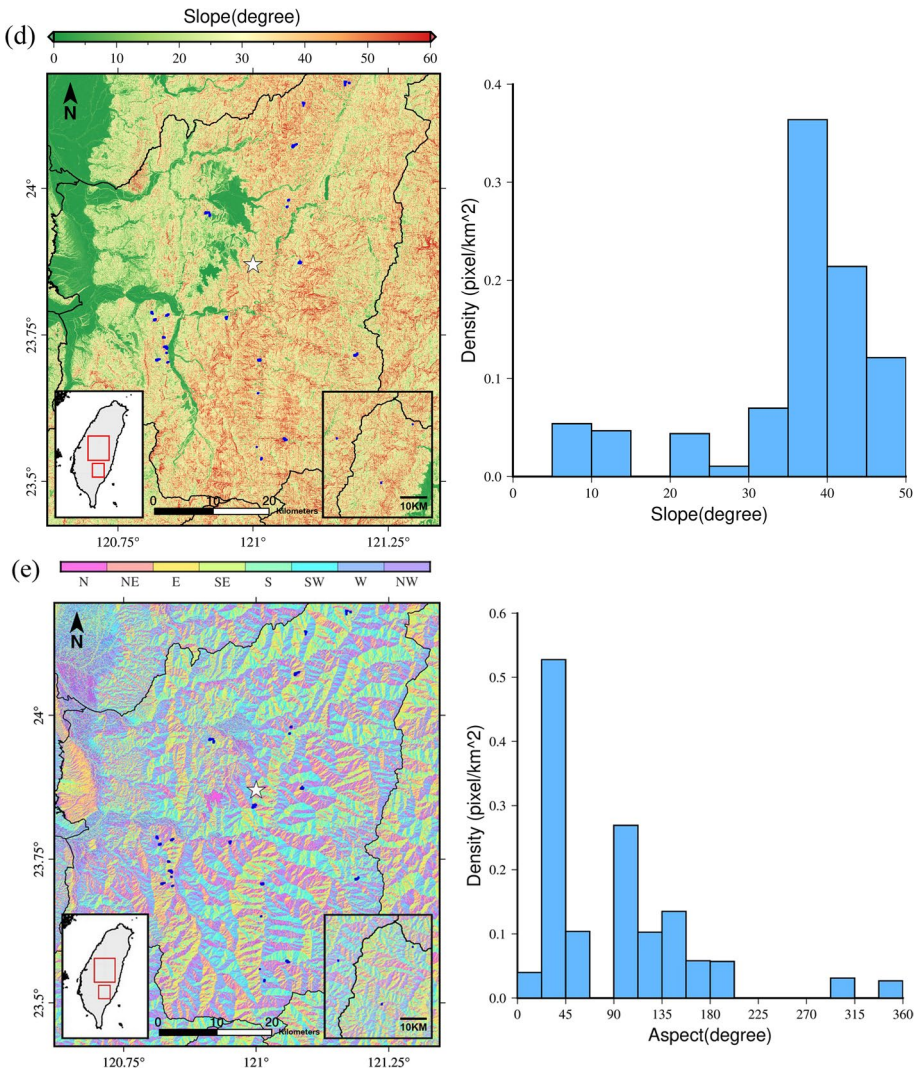

Fig. 2 continued

2000; Tanyaş and Lombardo 2019). The statistical results also reflected high PGA values between 0.35*g* and 0.5*g* had a high density of landslides, which is consistent with a high correlation between ground shaking and landslide occurrence (e.g., Chuang et al. 2021; Meunier et al. 2007; Nowicki et al. 2014).

Secondly, we generated the lithological data to ten rock types (Fig. 2b): Szeleng Sandstone and Paileng Formation (SLS), Hsitsun Formation (HT), Nankang Formation (NK), Kueichulin Formation (KCL), Toukoshan Formation (TKS), Lushan Formation (LS), Pilushan Formation (PLS), Tachien Sandstone (TC), Tananao Schist (TNA), and alluvium (AL). The landslide occurred within the formations around the epicenter, but did not show clear correlation with the specific formation. SLS and NK have higher landslide density, and TNA and AL have lower landslide density.

Thirdly, we classified the slope roughness layer and noticed a spatial pattern that landslides were mostly located at pixels with high values of slope and slope roughness (Fig. 2c, d). From the statistical analysis of slope roughness, a high density of landslides was found at slope roughness values greater than 40. The positive correlation between the landslide occurrence and slope roughness is consistent with the influence of high slope variations suggested by previous studies (Budimir et al. 2015; Chuang et al. 2021). Another factor, slope, also indicates a similar pattern. The high density of landslides is located at the slope between 35 and 50 degrees, which is similar to the analysis of the landslides of the Chi-Chi

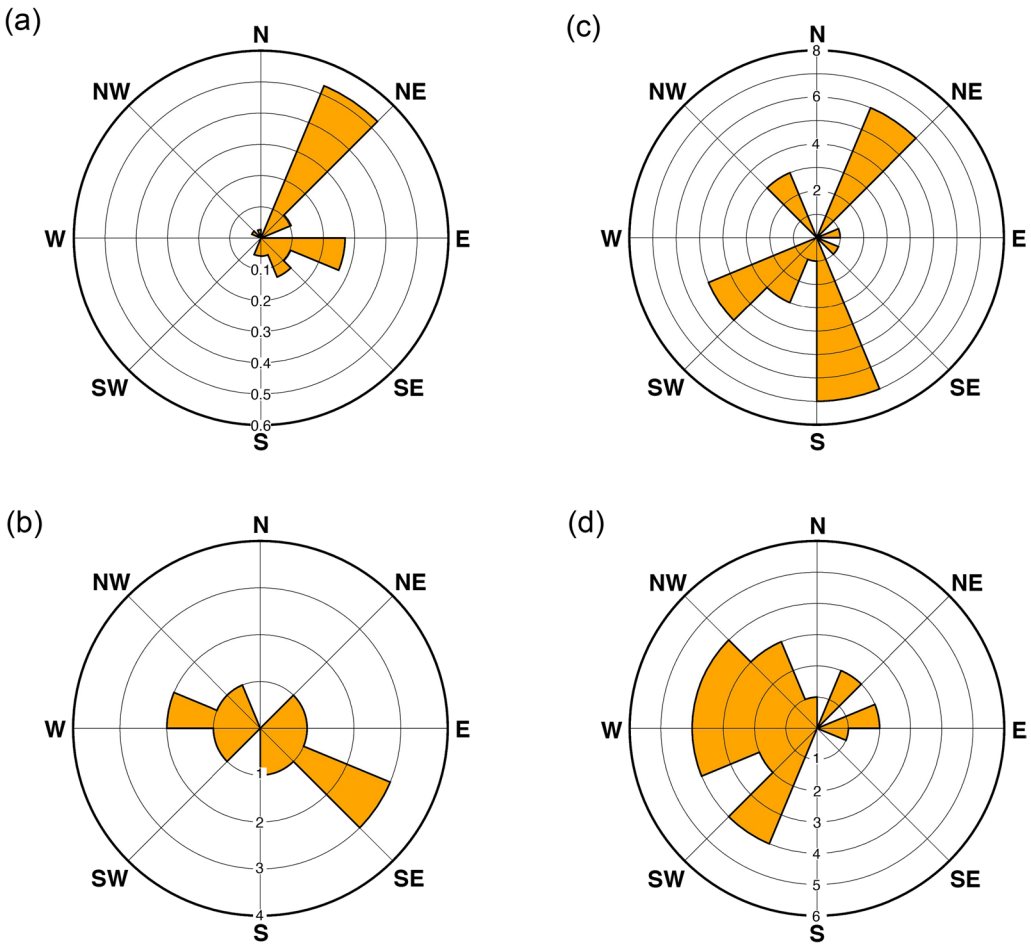

Fig. 3 Rose diagrams of **a** slope aspects, **b** dip directions, **c** wave propagation directions, and **d** surface displacement directions

earthquake (Khazai and Sitar 2004; Meunier et al. 2008). The slope below 30 degrees had a low density of landslides. The correlation between the landslides and high slope angles is also consistent with previous studies (Huang and Montgomery 2014; Huang et al. 2017).

Lastly, we used the DEM data to calculate an aspect layer and generated eight classes to represent eight sections of aspect directions. It was not intuitive to observe the spatial relationship between the aspects and landslides from the map. However, the statistical results revealed that the direction of the northeast had the highest density of landslides (Fig. 2e). A rose diagram further denotes that the main direction of the landslides is the northeast (Fig. 3a).

In summary, the above outcomes indicate that earthquake-triggered landslides had a high spatial relationship with the topological and seismic factors. From the analysis of the density of landslides and key factors, we also explored a strong correlation between landslides and certain classes within each factor.

Discussion

Seismic and geomorphic factors are two drivers leading to earthquake-triggered landslides in this study. Seismic factors primarily control the distribution and occurrence of earthquake-triggered landslides. Seismic factors, which describe the intensity of ground shaking and earthquake behaviors at surrounding localities near epicenters, are the most influential in earthquake-triggered landslides (Keefer 1994; Malamud et al. 2004; Meunier et al. 2007). Explicit factors representing the seismic shaking such as PGA and Arias intensity (Arias 1970) and implicit factors such as the distance to the epicenter and to fault rupture are highly related to the number of landslides, which is consistent with our result (Fig. 2a).

Geomorphic factors also control the earthquake-triggered landslides, and the landslide distribution shows a distinct pattern of the aspect directions. The slope is one major geomorphic factor controlling the distribution of earthquake-triggered landslides (e.g., Keefer 2002; Nowicki et al. 2014; Nowicki Jessee et al. 2018), and slope

roughness is also important for earthquake-triggered landslides in Taiwan (Budimir et al. 2015; Chuang et al. 2021; Lee et al. 2008). Based on our result, most of the landslides occurred on the east-facing slopes, especially in the northeastern direction, which means the landslides tend to occur in areas with higher values of slope and slope roughness (Fig. 2c, d).

The landslide aspects seem to be less associated with dip directions and seismic wave propagations. Since the landslides had a tendency of the aspects in the northeast directions (Fig. 3a), we compared this unique pattern with other directional factors. One possible factor is the dip directions of rocks because the dip slopes are prone to landslides (Khazai and Sitar 2004; Lin and Tung 2004). We obtained the dataset of the dip directions from the geology cloud data service at CGS (https://geologycloud.tw/geohome/DataService) and used the nearest dip direction for each landslide (Fig. 3b). The result shows that the dip directions of the rocks at the landslides are in the southeast and northwest, which do not fit the

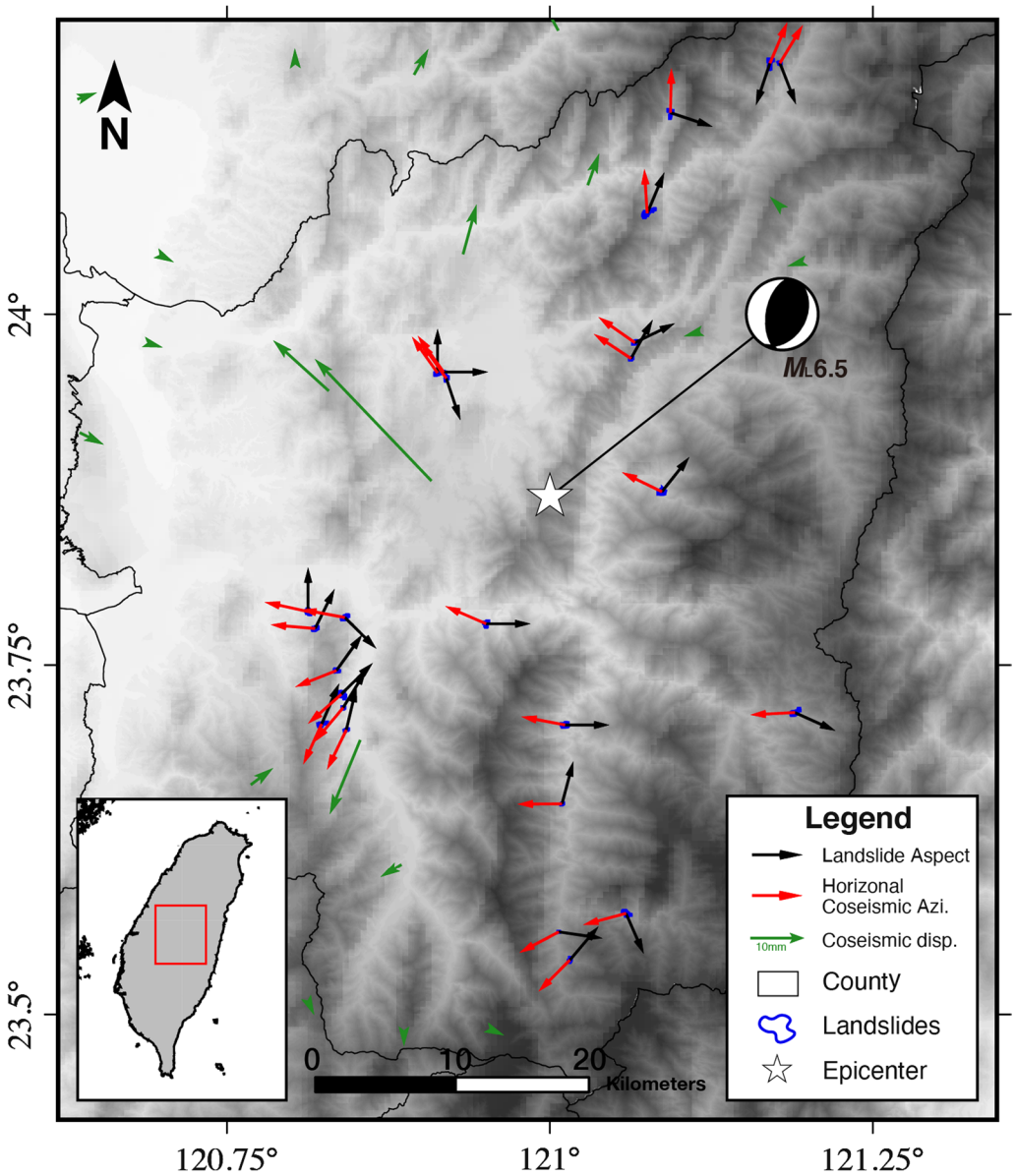

Fig. 4 Comparison between landslide aspects (black arrows) and the azimuths of horizontal coseismic displacement (red arrows) for the landslides induced by the 2013 M_L6.5 Nantou earthquake. White star denotes the epicenter. Small blue polygons are earthquake-triggered landslides. Black arrows are landslide aspects, red arrows are surface displacements at landslides, green arrows are observed coseismic displacements

landslide aspects. The disagreement between the landslide directions and the dip directions is similar to the situation of the Chi-Chi earthquake landslides (Chen et al. 2019). Another possible factor to control the aspect directions of earthquake-triggered landslides is the directions of seismic wave propagation that Earthquake-triggered landslides tend to occur on the slopes at the back sides of the wave propagation directions. (Chen et al. 2019; Meunier et al. 2008; Tibaldi et al. 1995). In this study, however, the seismic wave directions of the landslides show a radial pattern (Fig. 3c) and are not correlated with the landslide aspects.

Some of the landslide aspects seem to be in the opposite direction of the coseismic displacements. In addition to the seismic wave propagation, coseismic surface movements can be related to the landslide distributions (Kargel et al. 2016; Lee 2013). Because the Nantou earthquake occurred on a blind thrust without surface rupture (Chuang et al. 2013), all the landslides basically are located in the hanging-wall area (Fig. 1). Considering the focal mechanism solution (Fig. 1), the coseismic displacements should be in the west-southwest direction, which could be in the opposite direction with the landslide aspects. Therefore, we compared the landslide aspects to the directions of coseismic deformation. We used GPS observations of coseismic displacements (Chuang et al. 2013) to interpolate the horizontal displacement at each landslide location. Figures 3d, 4 show that the coseismic displacements are mainly towards southwest-west and facing away from the aspects, especially close to the epicenter. Especially, one group of the surface displacements is in the exact opposite direction of the northeastward landslide aspect. It seems that some landslides indeed are in the opposite directions of the surface displacements (Fig. 4). We calculated the included angles between the aspects and the displacement directions for all the landslides to quantify the deviation from the landslide aspects and surface displacements. Then, we compared the included angles with the distances to the epicenter. The included angles are ~100°–180° for all the landslides.

Coseismic displacements may affect the landslide distribution and orientation. Ground shaking due to seismic wave propagation can cause surface motion and result in slope instability. Intuitively, surface displacements due to coseismic deformation could be another ground motion source that can cause slope instability. Lee (2013) found that a lot of south- to southeast-facing landslides of the Chi-Chi earthquake may be associated with the northwestern movements on the hanging-wall area. Similar to Lee (2013), our result shows east-facing landslides may be also associated with the west–southwestward movements of the hanging-wall thrust block. Some factors control the occurrence of earthquake-triggered landslides such as coseismic slip patterns (e.g., Gorum et al. 2011; Meunier et al. 2013) and the distance to fault rupture (e.g., Budimir et al. 2014; Chigira et al. 2010; Lee 2013), which could be highly correlated with coseismic displacements, but they are interpreted to represent seismic intensity or seismic directivity rather than coseismic deformation. The total contribution of ground motion due to seismic shaking and coseismic deformation needs more further studies, and the specific ground-motion process in three dimensions at each earthquake-triggered landslide also needs more investigation.

Conclusion

We explored the spatial relationship between earthquake-triggered landslides and essential driving factors through the integration of remote sensing images and topographical properties of the 2013 M_L 6.5 Nantou earthquake. We mapped the landslides by using Landsat-8 images before and after the event and identified 30 large landslides. With the analysis between the landslides and major driving factors, we found that most of the landslides occurred within the area with high PGA, slope, and slope roughness. In addition, we discovered that the landslide aspects have a distinct pattern, showing a northeastward tendency. This pattern does not match the dip directions and seismic wave propagation at the landslides. We found that the directions of coseismic deformation had certain correlations with landslide aspects, and the relationship indicated that the coseismic deformation may play a role in landslide distribution. Thus, we successfully created the landslide inventory of a strong earthquake event in Taiwan and developed the analytical process to identify the spatial relationship between landslides and essential triggers.

Abbreviations

TWD97: Taiwan Geodetic Datum 1997; GRS80: Geodetic Reference System 1980; ITRF94: International Terrestrial Reference Frame 1994; CWB: Central Weather Bureau; PGA: Peak ground acceleration; CGS: Central Geological Survey; DEM: Digital elevation model; SLS: Szeleng Sandstone and Paileng Formation; HT: Hsitsun Formation; NK: Nankang Formation; KCL: Kueichulin Formation; TKS: Toukoshan Formation; LS: Lushan Formation; PLS: Pilushan Formation; TC: Tachien Sandstone; TNA: Tananao Schist; AL: Alluvium.

Supplementary Information

The online version contains supplementary material available at https://doi.org/10.1186/s40623-021-01560-8.

Additional file 1: Figure S1. Two-week daily precipitation prior to the M_L6.5 2013 Nantou earthquake at the weather station of Shuangdong near the epicenter.

Acknowledgements
We thank Dr. Nai-Chi Hsiao for providing technical supports. We thank the Central Weather Bureau for providing data. We thank US Geological Survey for providing Landsat imagery. We thank the Ministry of Interior for providing digital topographic data. The figures were generated using the Generic Mapping Tools (GMT) and ESRI ArcGIS.

Authors' contributions
BSW conducted data collection, processing, and analysis as well as paper writing. RYC initiated the study to form the conceptual idea and help paper writing. YCC helped improve the manuscript. YSL helped resources and figure modification. All authors have read and approved the final manuscript.

Authors' information
BS Wu is an assistant professor at Department of Geography, National Taiwan Normal University. RY Chuang is an associate professor at Department of Geography, National Taiwan University. YC Chen is an associate professor at Department of Geography, National Changhua University of Education. YS Lin is a research assistant at Department of Geography, National Taiwan University. All authors are members of the Geography Society of China Located in Taipei.

Funding
This research is supported by the Ministry of Science and Technology with project number of 107-2119-M-003-003-MY2 and 109-2116-M-002-011.

Availability of data and materials
The Landsat imagery used in this study is adopted from the USGS Earth Explorer website (https://earthexplorer.usgs.gov). The earthquake data used in this study are adopted from the Central Weather Bureau website (https://www.cwb.gov.tw).

Declarations

Ethics approval and consent to participate
Not applicable.

Consent for publication
Not applicable.

Competing interests
All the authors do not have any financial competing interests. None of the authors of this manuscript held any stocks, shares, and patents related to the content.

Author details
[1]Department of Geography, National Taiwan Normal University, Taipei, Taiwan. [2]Department of Geography, National Taiwan University, Taipei, Taiwan. [3]NTU Research Center for Future Earth, Taipei, Taiwan. [4]Department of Geography, National Changhua University of Education, Changhua City, Taiwan.

Received: 17 May 2021 Accepted: 12 December 2021
Published online: 04 January 2022

References

Arias A (1970) Measure of earthquake intensity. University of Chile, Santiago de Chile

Barlow J, Martin Y, Franklin SE (2003) Detecting translational landslide scars using segmentation of Landsat ETM+ and DEM data in the northern Cascade Mountains, British Columbia. Can J Remote Sens 29(4):510–517. https://doi.org/10.5589/m03-018

Budimir MEA, Atkinson PM, Lewis HG (2014) Seismically induced landslide hazard and exposure modelling in Southern California based on the 1994 Northridge, California earthquake event. Landslides 12:895–910. https://doi.org/10.1007/s10346-014-0531-8

Budimir MEA, Atkinson PM, Lewis HG (2015) A systematic review of landslide probability mapping using logistic regression. Landslide 12:419–436. https://doi.org/10.1007/s10346-014-0550-5

Central Geological Survey (2000) 1:500,000 Taiwan geological map. Central Geological Survey, the Ministry of Economic Affair, Taipei

Chan CH, Ma KF, Shyu JBH, Lee YT, Wang YJ, Gao JC, Yen YT, Rau RJ (2020) Probabilistic seismic hazard assessment for Taiwan: TEM PSHA2020. Earthq Spectra 36:137–159. https://doi.org/10.1177/8755293020951587

Chang KT, Chiang SH, Hsu ML (2007) Modeling typhoon- and earthquake-induced landslides in a mountainous watershed using logistic regression. Geomorphology 89:335–347. https://doi.org/10.1016/j.geomorph.2006.12.011

Chen YC, Chang KT, Wang SF, Huang JC, Yu CK, Tu JY, Chu HJ, Liu CC (2019) Controls of preferential orientation of earthquake and rainfall-triggered landslides in Taiwan's orogenic mountain belt. Earth Surf Process Landf 44:1661–1674. https://doi.org/10.1002/esp.4601

Cheng SN, Yeh YT, Hsu MT, Shin TC (1999) Photo album of ten disastrous earthquakes in Taiwan. Central Weather Bureau and Insitute of Earth Science, Academia Sinica, Taipei

Chigira M, Wu X, Inokuchi T, Wang G (2010) Landslides induced by the 2008 Wenchuan earthquake, Sichuan, China. Geomorphology 118:225–238. https://doi.org/10.1016/j.geomorph.2010.01.003

Chuang RY, Johnson KM, Wu YM, Ching KE, Kuo LC (2013) A midcrustal ramp-fault structure beneath the Taiwan tectonic wedge illuminated by the 2013 Nantou earthquake series. Geophys Res Lett 40:5080–5084. https://doi.org/10.1002/grl.51005

Chuang RY, Lu CH, Yang CJ, Lin YS, Lee TY (2020) Coseismic uplift of the 1999 *M*w7.6 Chi-Chi earthquake and implication to topographic change in frontal mountain belts. Geophys Res Lett 47:e2020GL088947. https://doi.org/10.1029/2020GL088947

Chuang RY, Wu BS, Liu HC, Huang HH, Lu CH (2021) Development of a statistics-based nowcasting model for earthquake-triggered landslides in Taiwan. Eng Geol 289:106177. https://doi.org/10.1016/j.enggeo.2021.106177

Dadson SJ, Hovius N, Chen H, Dade WB, Lin JC, Hsu ML, Lin CW, Horng MJ, Chen TC, Milliman J, Stark CP (2004) Earthquake-triggered increase in sediment delivery from an active mountain belt. Geology 32(8):733–736. https://doi.org/10.1130/G20639.1

Dai FC, Xu C, Yao X, Xu L, Tu XB, Gong QM (2011) Spatial distribution of landslides triggered by the 2008 M_s8.0 Wenchuan earthquake. China J Asian Earth Sci 40:883–895. https://doi.org/10.1016/j.jseaes.2010.04.010

Daniell JR, Schaefer AM, Wenzel F (2017) Losses associated with secondary effects in earthquakes. Front Built Environ 3:30. https://doi.org/10.3389/fbuil.2017.00030

Deijns AAJ, Bevington AR, van Zadelhoff F, de Jong SM, Geertsema M, McDougall S (2020) Semi-automated detection of landslide timing using harmonic modelling of satellite imagery, Buckinghorse River, Canada. Int J Appl Earth Obs Geoinf 84:101943. https://doi.org/10.1016/j.jag.2019.101943

Fan X, Scaringi G, Korup O, West AJ, van Wesen CJ, Tanyaş H, Hovius N, Hales TC, Jibson RW, Allstadt KE, Zhang L, Evans SG, Xu C, Li G, Pei X, Xu Q, Huang R (2019) Earthquake-induced chains of geologic hazards: patterns, mechanisms, and impacts. Rev Geophys 57(2):421–503. https://doi.org/10.1029/2018RG000626

Gorum T, Fan X, van Westen CJ, Huang RQ, Xu Q, Tang C, Wang G (2011) Distribution pattern of earthquake-induced landslides triggered by the 12 May 2008 Wenchuan earthquake. Geomorphology 133:152–167. https://doi.org/10.1016/j.geomorph.2010.12.030

Harp EL, Keefer DK, Sato HP, Yagi H (2011) Landslide inventories: the essential part of seismic hazard analyses. Eng Geol 122:9–12. https://doi.org/10.1016/j.enggeo.2010.06.013

Hovius N, Maunier P, Lin CW, Chen H, Chen YG, Dadson S, Horng MJ, Lines M (2011) Prolonged seismically induced erosion and the mass balance of a large earthquake. Earth Planet Sci Lett 304:347–355. https://doi.org/10.1016/j.eps.2011.02.005

Hsiao NC (2007) Establishment of ground motion prediction model. Report CWB96-1A-06. Central Weather Bureau Research, Taiwan

Huang TF, Lee CT (1999) Landslides triggered by the Jueili earthquake. Proceedings of the 1999 Annual Meeting of the Geological Society of China, Taipei

Huang AYL, Montgomery DR (2014) Topographic locations and size of earthquake- and typhoon-generated landslides, Tachia River. Taiwan Earth Surf Process Landf 39:414–418. https://doi.org/10.1002/esp.3510

Huang JC, Milliman JD, Lee TY, Chen YC, Lee JF, Liu CC, Lin JC, Kao SJ (2017) Terrain attributes of earthquake- and rainstorm-induced landslides in orogenic mountain belt. Taiwan Earth Surf Process Landf 42:1549–1559. https://doi.org/10.1002/esp.4112

Kargel JS, Leonard GJ, Shugar DH, Haritashya UK, Bevington A, Fielding EJ, Fujita K, Geertsema M, Miles ES, Steiner J, Anderson E, Bajracharya S, Bawden GW, Breashears DF, Byers A, Collins B, Dhital MR, Donnellan A, Evans TL, Geai ML, Glasscoe MT, Green D, Gurung DR, Heijenk R, Hilborn A, Hudnut K, Huyck C, Immerzeel WW, Liming J, Jibson R, Kaab A, Khanal NR, Kirschbaum D, Kraaijenbrink PDA, Lamsal D, Shiyin L, Mingyang L, McKinney D, Nahirnick NK, Zhuotong N, Ojha S, Olsenholler J, Painter TH, Pleasants M, Pratima KC, Yuan QI, Raup BH, Regmi D, Rounce DR, Sakai A, Donghui S, Shea JM, Shrestha AB, Shukla A, Stumm D, van der Kooij M, Voss K, Xin W, Weihs B, Wolfe D, Lizong W, Xiaojun Y, Yoder MR, Young N (2016) Geomorphic and geologic controls of gehazards induced by Nepal's 2015 Gorkha earthquake. Science 351(6269):aac8353. https://doi.org/10.1126/science.aac8353

Keefer DK (1984) Landslides caused by earthquakes. Geol Soc Am Bull 95:406–421. https://doi.org/10.1023/A:1021274710840

Keefer DK (1994) The importantce of earthquake-induced landslides to long-term slope erosion and slope failure hazards in seismically active regions. Geology 10:265–285. https://doi.org/10.1016/B978-0-444-82012-9.50022-0

Keefer DK (2002) Investigating landslides caused by earthquakes—a historical review. Surv Geophys 23:473–510. https://doi.org/10.1023/A:1021274710840

Khazai B, Sitar N (2004) Evaluation of factors controlling earthquake-induced landslides caused by Chi-Chi earthquake and comparison with Northridge and Loma Prieta events. Eng Geol 71:79–95. https://doi.org/10.1016/S0013-7952(03)00127-3

Larsen IJ, Montgomery DR, Korup O (2010) Landslide erosion controlled by hillslope material. Nat Geosci 3:247–251. https://doi.org/10.1038/ngeo776

Lee CT (2013) Re-evaluation of factors controlling landslides triggered by the 1999 Chi-Chi earthquake. In: Ugai K, Yagi H, Wakai A (eds) Earthquake-induced landslides. Springer, Berlin, pp 213–224

Lee CT, Fei LY (2015) Nationwide landslide hazard analysis and mapping in Taiwan. Eng Geology Soc Territ 2:971–974. https://doi.org/10.1007/978-3-319-09057-3_169

Lee CT, Huang CC, Lee JF, Pan KL, Lin ML, Dong JJ (2008) Statistical approach to earthquake-induced landslide susceptibility. Eng Geology 100:43–58. https://doi.org/10.1016/j.enggeo.2008.03.004

Lee SJ, Yeh TY, Huang HH, Lin CH (2015) Numerical earthquake models of the 2013 Nantou, Taiwan, earthquake series: characteristics of source rupture processes, strong ground motions and their tectonic implication. J Asian Earth Sci 111:365–372. https://doi.org/10.1016/j.jseaes.2015.06.031

Liao HW, Lee CT (2000) Landslide triggered by the Chi-Chi earthquake. Proceedings of the 21st Asian Conference on Remote Sensing, Taipei

Lin ML, Tung CC (2004) A GIS-based potential analysis of the landslides induced by the Chi-Chi earthquake. Eng Geol 71:63–77. https://doi.org/10.1016/S0013-7952(03)00126-1

Lin SC, Ke MC, Lo CM (2017) Evolution of landslide hotspots in Taiwan. Landslides 14:1491–1501. https://doi.org/10.1007/s10346-017-0816-9

Malamud BD, Turcotte DL, Guzzetti F, Reichenbach P (2004) Landslide, earthquakes, and erosion. Earth Planet Sci Lett 229:45–59. https://doi.org/10.1016/j.epsl.2004.10.018

Mantovani F, Soeters R, Van Westen CJ (1996) Remote sensing techniques for landslide studies and hazard zonation in Europe. Geomorphology 15(3):213–225. https://doi.org/10.1016/0169-555X(95)00071-C

Marano KD, Wald DJ, Allen TI (2009) Global earthquake casualties due to secondary effects: a quantitative analysis for improving rapid loss analyses. Nat Hazards 52(2):319–328. https://doi.org/10.1007/s11069-009-9372-5

Marc O, Hovius N, Meunier P, Uchida T, Hayashi S (2015) Transient changes of landslide rates after earthquakes. Geology 43:883–886. https://doi.org/10.1130/G36961.1

Marcelino EV, Formaggio AR, Maeda EE (2009) Landslide inventory using image fusion techniques in Brazil. Int J Appl Earth Obs Geoinf 11(3):181–191. https://doi.org/10.1016/j.jag.2009.01.003

Meunier P, Hovius N, Haines AJ (2007) Regional patterns of earthquake-triggered landslides and their relation to ground motion. Geophys Res Lett 34:L20408. https://doi.org/10.1029/2007GL031337

Meunier P, Hovius N, Haines JA (2008) Topographic site effects and the location of earthquake induced landslides. Earth Planet Sci Lett 275:221–232. https://doi.org/10.1016/j.espl.2008.07.020

Meunier P, Uchida T, Hovius N (2013) Landslide patterns reveal the sources of large earthquakes. Earth Planet Sci Lett 363:27–33. https://doi.org/10.1016/j.epsl.2012.12.018

Nadim F, Kjekstad O, Peduzzi P, Herold C, Jaedicke C (2006) Global landslide and avalanche hotspot. Landslides 3(2):159–173. https://doi.org/10.1007/s10346-006-0036-1

Nowicki MA, Wald DJ, Hamburger MW, Hearne M, Thompson EM (2014) Development of a globally applicable model for near real-time prediction of seismically induced landslides. Eng Geol 173:54–65. https://doi.org/10.1016/j.enggeo.2014.02.002

Nowicki Jessee MA, Hamburger MW, Allstadt K, Wald DJ, Robeson SM, Tanyaş H, Hearne M, Thompson EM (2018) A global empirical model for near-real-time assessment of seismically induced landslides. J Geophys Res Earth Surface 123:1835–1859. https://doi.org/10.1029/2017JF004494

Nowicki Jessee MA, Hamburger MW, Rerrara MR, McLean A, FitzGerald C (2020) A global dataset and model of earthquake-induced landslide fatalities. Landslides 17:1363–1376. https://doi.org/10.1007/s10346-020-01356-z

Rodriguez CE, Bommer JJ, Chandler RJ (1999) Earthquake-induced landslides: 1980–1997. Soil Dyn Earthq Eng 18:325–346. https://doi.org/10.1016/S0267-7261(99)00012-3

Sato HP, Hasegawa H, Fujiwara S, Tobita M, Koarai M, Une H, Iwahashi J (2007) Interpretation of landslide distribution triggered by the 2005 Northern Pakistan earthquake using SPOT 5 imagery. Landslides 4:113–122. https://doi.org/10.1007/s10346-006-0069-5

Schimitt RG, Tanyaş H, Nowicki Jessee MA, Zhu J, Biegel KM, Allstadt KE, Jibson RW, Thompson EM, van Westen CJ, Sato HP, Wald DJ, Godt JW, Gorum T, Xu C, Rathje EM, Knudsen KL (2017) An open repository of earthquake-triggered ground-failure inventories. US Geological Survey Data Series, 1064, Reston, p 17. https://doi.org/10.3133/ds1064

Shyu JBH, Sieh K, Chen YG, Liu CS (2005) Neotectonic architecture of Taiwan and its implications for future large earthquakes. J Geophys Res 110:B08402. https://doi.org/10.1029/2004JB003251

Shyu JBH, Yin YH, Chen CH, Chuang YR, Liu SC (2020) Updates to the on-land seismogenic structure source database by the Taiwan Earthquake Model (TEM) project for seismic hazard analysis of Taiwan. Terr Atmos Ocean Sci 31:469–478. https://doi.org/10.3319/TAO.2015.11.27.02

Tanyaş H, Lombardo L (2019) Variation in landslide-affected area under the control of ground motion and topography. Eng Geol 260:105229. https://doi.org/10.1016/j.enggeo.2019.105229

Tanyaş H, van Westen CJ, Allstadt KE, Nowicki Jessee MA, Görüm T, Jibson RW, Godt JW, Sato HP, Schimitt RG, Marc O, Hovius N (2017) Presentation and analysis of a worldwide database of earthquake-induced landslide inventories. J Geophys Res Earth Surf 122:1991–2015. https://doi.org/10.1002/2017JF004236

Tibaldi A, Ferrari L, Pasquare G (1995) Landslides triggered by earthquakes and their relations with faults and mountain slope geometry: an example from Ecuador. Geomorphology 11:215–226. https://doi.org/10.1016/0169-555X(94)00060-5

van Westen CJ, van Asch TWJ, Soeters R (2006) Landslide hazard and risk zonation-why is it still so difficult? Bull Eng Geol Env 65:167–184. https://doi.org/10.1007/s10064-005-0023-0

Wen YY, Miyake H, Yen YT, Irikura K, Ching KE (2014) Rupture directivity effect and stress heterogeneity of the 2013 Nantou blind-thrust earthquakes. Taiwan Bull Seismo Soc Am 104:2933–2942. https://doi.org/10.1785/0120140109

Wu YM, Chang CH, Zhao L, Teng TL, Nakamura M (2008) A comprehensive relocation of earthquakes in Taiwan from 1991 to 2005. Bull Seismo Soc Am 98:1471–1481. https://doi.org/10.1785/0120070166

Yagi H, Sato G, Higaki D, Yamamoto M, Yamasaki T (2009) Distribution and characteristics of landslides induced by the Iwate-Miyagi Nairiku Earthquake in 2008 in Tohoku District, Northeast Japan. Landslides 6:335. https://doi.org/10.1007/s10346-009-0182-3

Yang M, Tseng CL, Yu JY (2001) Establishment and maintenance of Taiwan geodetic datum 1997. J Surv Eng 127(4):119–132. https://doi.org/10.1061/(ASCE)0733-9453(2001)127:4(119)

Yu B, Chen F, Xu C (2020) Landslide detection based on contour-based deep learning framework in case of national scale of Nepal in 2015. Comput Geosci 135:104388. https://doi.org/10.1016/j.cageo.2019.104388

Zhao B, Li W, Wang Y, Lu J, Li X (2019) Landslides triggered by the Ms 6.9 Nyingchi earthquake, China (18 November 2017): analysis of the spatial distribution and occurrence factors. Landslides 16:765–776. https://doi.org/10.1007/s10346-019-01146-2

Publisher's Note